

Quantum Telecloning on NISQ Computers

Elijah Pelofske^{*1}, Andreas Bäertschi^{†1}, Bryan Garcia², Boris Kiefer², and Stephan Eidenbenz¹

¹CCS-3 Information Sciences, Los Alamos National Laboratory

²Department of Physics, New Mexico State University

Abstract

Due to the no-cloning theorem, generating perfect quantum clones of an arbitrary quantum state is not possible, however approximate quantum clones can be constructed. Quantum telecloning is a protocol that originates from a combination of quantum teleportation and quantum cloning. Here we present $1 \rightarrow 2$ and $1 \rightarrow 3$ quantum telecloning circuits, with and without ancilla, that are theoretically optimal (meaning the clones are the highest fidelity allowed by quantum mechanics), universal (meaning the clone fidelity is independent of the state being cloned), and symmetric (meaning the clones all have the same fidelity). We implement these circuits on gate model IBMQ and Quantinuum NISQ hardware and quantify the clone fidelities using parallel single qubit state tomography. Quantum telecloning using mid-circuit measurement with real time if statements is demonstrated on the Quantinuum H1-2 device. Two alternative implementations of quantum telecloning (deferred measurement and post selection) are demonstrated on `ibmq_montreal` for cases where mid-circuit measurement with real time if statements are not available. Our results show that NISQ devices can achieve near-optimal quantum telecloning fidelity; for example the Quantinuum H1-2 device running the telecloning circuits without ancilla achieved a mean clone fidelity of 0.824 for two clone circuits and 0.765 for three clone circuits (the theoretical fidelity limits are 0.833 for two clones and 0.77 for three clones). This demonstrates the viability of performing experimental analysis of quantum information networks and quantum cryptography protocols on NISQ computers.

Keywords: Quantum computing, Quantum telecloning, telecloning, NISQ computers, Parallel state tomography, quantum cloning, measurement error mitigation, Mid-circuit measurement and real time conditional operations, Qiskit

1 Introduction

The concepts of quantum mechanics allow for non-classical information processing approaches especially due to superposition [20], and entangled states [27]. However, probability as a foundational pillar of quantum mechanics suggests that some concepts of classical deterministic information processing cannot be transferred. An example is the no-cloning theorem [47], which states that due to the linearity of quantum mechanics, an arbitrary quantum state cannot be perfectly cloned, with the corollary that the laws of quantum mechanics preclude eavesdropping on quantum communication [4]. However, the no-cloning theorem does not preclude probabilistic perfect cloning [19,35] or deterministic optimal cloning [10]. The latter generates M optimal clones from N identical input states through a unitary Quantum Cloning Machine (QCM) [23]. QCM's are characterized by an entangled multipartite state which can play the role of a quantum network for the distribution of quantum information [11]. Due to their maximal entanglement [3] and robustness to decoherence [24], Dicke states are a suitable choice for quantum networking protocols [16]. In quantum information science, Dicke states [18] form a family of highly-entangled multipartite quantum states, defined as the equal-weight superposition of all n -qubit states $|x\rangle$ with Hamming weight $\text{hw}(x) = i$ [12].

A convenient classification for optimal cloning and telecloning protocols is given by the *fidelity* of the clones with respect to the prepared pure quantum state [26,30]. In conjunction with quantum teleportation [5], which relies on local operations and classical communication (LOCC) of a Bell state measurement, optimal cloning can distribute M optimal clones of a 1-qubit quantum state to multiple recipients. **Optimal** telecloning generates clones with the maximum fidelity allowed by quantum mechanics [30].

*epelofske@lanl.gov

†baertschi@lanl.gov

Using state fidelity we can distinguish between **universal** quantum cloning [10] for which every input state is copied with equal fidelity, and state-dependent cloning [7] where the fidelity of the output clones depends on the state being cloned. Telecloning protocols that utilize a universal cloning machine have been developed for $1 \rightarrow 2$ telecloning [30], [49] and $1 \rightarrow 3$ telecloning [8]. State-dependent $1 \rightarrow 3$ telecloning has been realized in photonic quantum computing platforms with almost ideal fidelities for given input states [16]. In addition to the aforementioned QCM’s, we can distinguish between **symmetric** quantum cloning [6] where all clones have equal fidelity, and asymmetric cloning [25, 34] which outputs clones of different fidelity. Symmetric quantum telecloning of $0 \leq N \leq 30$ unknown spin states has been experimentally implemented with a maximum average fidelity of $F \approx 0.80$ for $N = 1$ and $M = 2$ [38], compared to the theoretical value of $F = 0.833$. Asymmetrical telecloning protocols have been developed for $1 \rightarrow 2$ telecloning of single-qubit states [31] and multi-qubit states [15], and have been realized in photonic quantum computing architectures with fidelities of $F \approx 0.88$ [48] (here the optimal fidelity is given by the no-cloning inequality [14]). We can further distinguish between quantum cloning with the quantum computing qubit model and quantum computing with continuous-variables [29]. This scheme consists of cloning variables with a continuous spectrum, such as position and momentum [13]. The extension to continuous-variable telecloning of $1 \rightarrow M$ optimal symmetric clones was later introduced [44]. Recently, $1 \rightarrow 3$ continuous-variable telecloning has been experimentally demonstrated [45].

In general, for M clones of N 1-qubit quantum states (where $M > N$) the optimal fidelity bound of the clones can be rigorously computed [30, 40]:

$$F_{N \rightarrow M} = \frac{MN + M + N}{M(N + 2)} \quad (1)$$

Here we consider telecloning of a single input state ($N = 1$). The optimal fidelities for $1 \rightarrow 2$ and $1 \rightarrow 3$ telecloning are $\frac{5}{6}$ (0.833) and $\frac{7}{9}$ (0.777), respectively.

We build on previous work: $1 \rightarrow 2$ optimal symmetric universal cloning [10], $1 \rightarrow 2$ telecloning without ancilla qubits [7], generalizations of $1 \rightarrow M$ and $N \rightarrow M$ cloning with ancilla [23], and $1 \rightarrow M$ telecloning with ancilla [30]. In these cases telecloning is based on a Bell measurement of the message and port qubit, followed by classically communicated controls for Pauli X/Z operations on the clones. The $1 \rightarrow 2$ ancilla-free telecloning protocol of [7] has shown that clone fidelities are dependent on the Bell measurement outcome of the message and port qubits. In contrast, the telecloning scheme [30] uses ancilla qubits to produce symmetric mixed states (the clones) and fidelities independent of the Bell measurement outcome. The scheme relies on a superposition of entangled Dicke states that act as a QCM, or *telecloning state*.

As our main contributions, we implement and thoroughly test $1 \rightarrow 2$ and $1 \rightarrow 3$ *optimal symmetric universal* quantum telecloning, with and without ancilla, on two distinct gate model qubit based Noisy Intermediate-Scale Quantum (NISQ) [37] computing commercial platforms. For $1 \rightarrow 3$ *optimal symmetric universal* quantum telecloning, we design a novel circuit without ancilla qubits that we use in our tests. We also present a concrete algorithm for generating $1 \rightarrow M$ quantum telecloning circuits with ancillas for $M \geq 2$. In Section 2.1 we present a unified algorithm for generating the $1 \rightarrow 2$ and $1 \rightarrow 3$ telecloning gate model circuits, with and without ancilla.

1. **$1 \rightarrow 2$ Telecloning without ancilla on ibmq_montreal-** The average clone fidelity for post selection with measurement error mitigation is 0.808.
2. **$1 \rightarrow 2$ Telecloning with ancilla on ibmq_montreal-** The average clone fidelity for post selection with measurement error mitigation is 0.731.
3. **$1 \rightarrow 3$ Telecloning without ancilla on ibmq_montreal-** The average clone fidelity for post selection with measurement error mitigation is 0.687.
4. **$1 \rightarrow 3$ Telecloning with ancilla on ibmq_montreal-** The average clone fidelity for post selection with measurement error mitigation is 0.629.
5. **Mid-circuit measurement with conditional operations on Quantinuum H1-2-** Telecloning circuits without ancilla achieved the best results with an average clone fidelity of 0.824 and 0.765 for two and three clones, respectively.

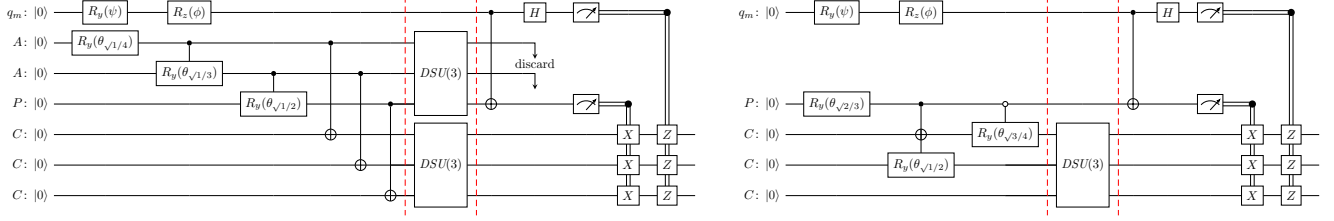


Figure 1: Two quantum telecloning circuits for three clones, with and without the use of ancilla for the telecloning states. We use little-endian ket notation (top-to-bottom wires correspond to left-to-right bitstrings) and shorthand angle notation $\theta_{\sqrt{x/y}} = 2 \cos^{-1}(\sqrt{x/y})$ such that $R_y(\theta_{\sqrt{x/y}}) |0\rangle = \sqrt{\frac{x}{y}} |0\rangle + \sqrt{\frac{y-x}{y}} |1\rangle$:

(left) Using an AAPCCC telecloning state (2 ancilla qubits A , 1 port qubit P , $M = 3$ clone qubits C): First prepare the message qubit on the top wire, and the state $\frac{1}{\sqrt{M}} \sum_{i=0}^M |1^i 0^{M-i}\rangle |1^i 0^{M-i}\rangle$. Symmetrize AAP and CCC using two Dicke state unitaries $DSU(M)$ to get $\frac{1}{\sqrt{M}} \sum_{i=0}^M |D_i^M\rangle |D_i^M\rangle$. Discard the ancilla qubits, perform a Bell measurement on the message and port qubits, and classically communicate the results to the holders of the clone qubits for them to control Pauli-X and Pauli-Z adjustments, similar to quantum teleportation.

(right) Using a PCCC telecloning state instead (1 port P , $M = 3$ clones C): Prepare $\sqrt{\frac{2}{3}} |0\rangle (\sqrt{\frac{3}{4}} |000\rangle + \sqrt{\frac{1}{4}} |100\rangle) + \sqrt{\frac{1}{3}} |1\rangle (\sqrt{\frac{1}{2}} |100\rangle + \sqrt{\frac{1}{2}} |110\rangle)$. Symmetrize the clone qubits CCC using a single Dicke state unitary $DSU(3)$ to get the state $\sqrt{\frac{1}{2}} |0\rangle |D_0^3\rangle + \sqrt{\frac{1}{6}} |0\rangle |D_1^3\rangle + \sqrt{\frac{1}{6}} |1\rangle |D_1^3\rangle + \sqrt{\frac{1}{6}} |1\rangle |D_2^3\rangle$. Perform a Bell measurement on the message and port qubits, followed by classical communication to and local Pauli operations on the clone qubits.

2 Methods

In this section we first detail the algorithmic circuit construction for the quantum telecloning circuits. This includes the circuit construction using different hardware connectivities. In Section 2.1 we detail the three different implementations of quantum telecloning; deferred measurement, post selection, and mid-circuit measurement with real time conditional operations. Lastly, in Section 2.2 we describe the state tomography estimation method used and the hardware dependent circuit execution parameters used.

2.1 Quantum Telecloning Protocol and Circuits

We begin by noting some key features of the quantum telecloning protocol. The teleportation component of telecloning enables the transmission of quantum information through a Bell state [22] measurement. The four Bell states are 2-qubit entangled quantum states that form a maximally entangled basis, here defined as $|\text{port,message}\rangle$:

$$\begin{aligned} \Phi^+ &: \frac{1}{\sqrt{2}}(|00\rangle + |11\rangle) & \Phi^- &: \frac{1}{\sqrt{2}}(|00\rangle - |11\rangle) \\ \Psi^+ &: \frac{1}{\sqrt{2}}(|01\rangle + |10\rangle) & \Psi^- &: \frac{1}{\sqrt{2}}(|01\rangle - |10\rangle) \end{aligned}$$

Another important yet subtle feature of the quantum telecloning protocol (see Algorithm 1) is that the message qubit, the telecloning state, and the resulting clones do not need to be spatially connected at all times. In particular, the relevant operation is the bell measurement on the message qubit by the telecloning state which subsequently generates the clones, meaning that the message qubit does not need to be initialized within the same proximity as the telecloning state. Another principal feature is the structure of the telecloning state, which plays two key roles, it produces optimal clones, and acts as a quantum channel to distribute the quantum information. We wish for this distribution of information to be symmetric between the clones, therefore, a fitting choice for this telecloning state are Dicke states, which contain the necessary entanglement and are symmetric under permutation of qubits (e.g., port and ancilla qubits) [9]. We construct telecloning states (illustrated in a quantikz [28] circuit in Figure 1 for three clones with and without ancilla) using Dicke state unitaries $DSU(M)$ [1, 12], defined as unitaries mapping any input Hamming weight i in unary encoding to the Dicke state $|D_i^M\rangle$:

$$\forall 0 \leq i \leq M: DSU(M) |1^i 0^{M-i}\rangle \mapsto |D_i^M\rangle$$

where the Dicke states $|D_i^M\rangle$ are a superposition of bitstrings x of length M of Hamming weight (number of ones)

Algorithm 1 Quantum telecloning protocol for cloning of $N = 1$ quantum state to $M > N$ clones

State Preparation:

- 1: A message qubit q_m is prepared by a sender
- 2: A quantum telecloning state TC is constructed with
 - 1 Port qubit, and potentially $M - 1$ ancilla qubits.
 - M clone qubits (sent to the receivers) plus TC is symmetric in the clones, and symmetric between the port and ancilla qubits (i.e. they are interchangeable).

Teleportation:

- 3: A bell measurement is made between q_m and the Port qubit of TC , and the results are communicated classically to the clone holders.
- 4: The clone holders use the result of the bell measurement to decide whether to apply X - and/or Z -gates to the clone qubits in order to construct the approximate clones:
 - Φ^+ : apply nothing
 - Φ^- : apply Z -gate
 - Ψ^+ : apply X -gate
 - Ψ^- : apply X - then Z -gate

Result:

- 5: M approximate clones of q_m have been generated with maximal fidelity described by Equation 1
-

$hw(x) = i$:

$$|D_i^M\rangle = \binom{M}{i}^{-\frac{1}{2}} \sum_{x \in \{0,1\}^M, hw(x)=i} |x\rangle$$

For $1 \rightarrow M$ telecloning with ancilla, the telecloning state is composed of $M - 1$ ancilla qubits, 1 port qubit, and M clone qubits, given by:

$$\sqrt{\frac{1}{M}} \sum_{i=0}^M |D_i^M\rangle |D_i^M\rangle$$

For $1 \rightarrow 2$ telecloning circuits without ancilla, the state is composed of 1 port qubit and 2 clone qubits:

$$\sqrt{\frac{2}{3}} |0\rangle |D_0^2\rangle + \sqrt{\frac{1}{3}} |1\rangle |D_1^2\rangle$$

Lastly, for $1 \rightarrow 3$ telecloning circuits without ancilla, the state consists of 1 port qubit and 3 clone qubits, novel for symmetric universal telecloning:

$$\sqrt{\frac{1}{2}} |0\rangle |D_0^3\rangle + \sqrt{\frac{1}{6}} |0\rangle |D_1^3\rangle + \sqrt{\frac{1}{6}} |1\rangle |D_1^3\rangle + \sqrt{\frac{1}{6}} |1\rangle |D_2^3\rangle$$

In order to emulate the quantum telecloning protocol on a NISQ computer, the important mechanism is how to use the bell measurement (classical) information to generate the clones. In order to do this the NISQ device would need to execute *mid-circuit measurement with subsequent classical control features* (i.e. if statements) to execute X/Z Pauli gates which then create approximate clones of the message qubit. This feature is available on the Quantinuum H1-2 device [36], which allows direct emulation of the quantum telecloning protocol. On the IBMQ hardware this is not currently supported. Therefore we present two alternative methods: *deferred measurement* and *post selection*.

The first alternative method, *deferred measurement*, is where instead of using the classical control to make decisions on what quantum operations to then apply, all of the control is done using quantum gates [33]. This has the advantage of removing the requirement of using classical control operations to perform the required bell measurement and then execute Pauli X/Z gates in order to generate the clones. The primary disadvantage of this mechanism is that it costs more CNOT's to implement.

The second alternative method, *post selection*, is where the X and / or Z Pauli gates are applied a priori (i.e. to all circuits) during the circuit execution; and then subsequently all measured states that do not correspond to that quantum control logic are removed during post processing. This is then repeated for all of the possible measured classical states of the port and message qubits (i.e. 11, 10, 01, 00). Therefore, 4 separate quantum circuits are executed (for a given message qubit) in order to implement post selection, and each of those runs will discard many

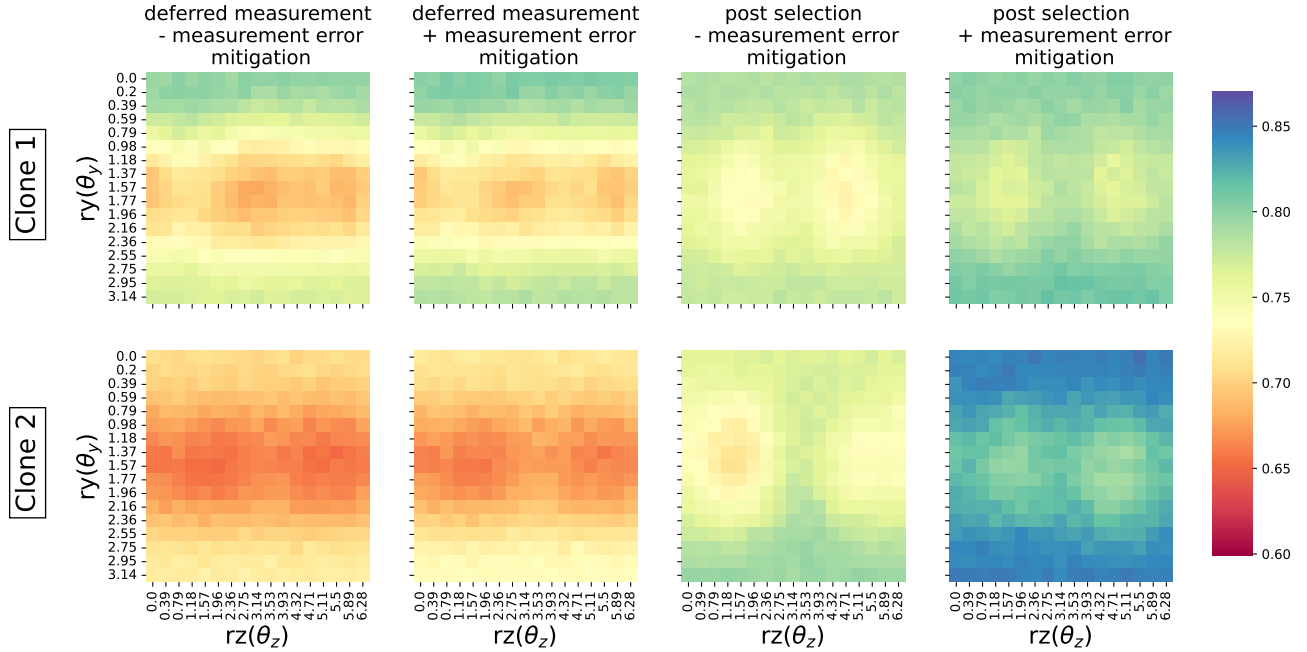


Figure 2: PCC circuit implemented in the form of deferred measurement and post selection of `ibmq_montreal`. The maximum fidelity is 0.833. First and third column show the raw fidelity results without measurement error mitigation, and the second and fourth columns show the same results with measurement error mitigation applied. Run on qubits **0, 1, 4, 7** on `ibmq_montreal`. The qubit clone indices, for the logical circuit, are 0, 2 for PCC deferred measurement and 2, 3 for PCC using post selection. The clone numbering on the rows corresponds to this numbering order (in other words the clone number is index based).

of the measured results. The primary downside with this method is that it requires the execution of 4 separate circuits for each telecloning circuit.

We define the telecloning circuit names using the following convention: **P** indicates the port qubit, **A** indicates an ancilla qubit, and **C** indicates a clone qubit. Thus, a combination of these letters encodes the circuit construction; for example `AAPCCC` indicates a telecloning circuit which uses two ancilla, one port, and creates three clone qubits. Note that in this naming convention, the *message* qubit is implicitly included because it is the state that is cloned.

We give circuit constructions for two underlying NISQ computer architectures; full all-to-all connectivity (Quantinuum compatible) and LNN connectivity between qubits of the Telecloning state + edge between Message & Port qubits (IBMQ compatible).

Among the available quantum operations on NISQ devices, two qubit gates and measurement have the highest error rates. Therefore next we summarize CNOT costs of our circuits in terms of the number of clones M (see Figure 1).

In order to prepare the initial telecloning state with ancilla (the portion of the circuit before the first vertical red line on the left hand sub diagram of Figure 1) it costs $2M^2 - M$ CNOTs on LNN connectivity and $2M - 1$ CNOTs on all-to-all connectivity.

In order to prepare the initial telecloning state with no ancilla (the portion of the circuit before the first vertical red line on the right hand sub diagram of Figure 1) it costs 1 CNOT for two clones (regardless of connectivity), 2 CNOTs for three clones on full connectivity, and 3 CNOTs for three clones on LNN connectivity.

Next, the Dicke state unitary preparation costs $2.5M^2 - 5.5M + 3$ per unitary [1]. With ancilla, the preparation requires two Dicke state unitaries whereas without ancilla it requires only a single Dicke state unitary (see Figure 1).

The bell measurement always uses exactly one CNOT gate across all circuits.

Deferred measurement requires additional CNOT gates whereas post selection and mid-circuit measurement with real time conditionals both require no additional CNOTs in order to implement LOCC. Deferred measurement costs $4M - 1$ CNOT's on LNN connectivity, and $2M$ CNOTs on full connectivity (note however that we do not run experiments with deferred measurement on full connectivity).

Thus using the template in Figure 1 the CNOT cost of all of our implementation of quantum telecloning circuits

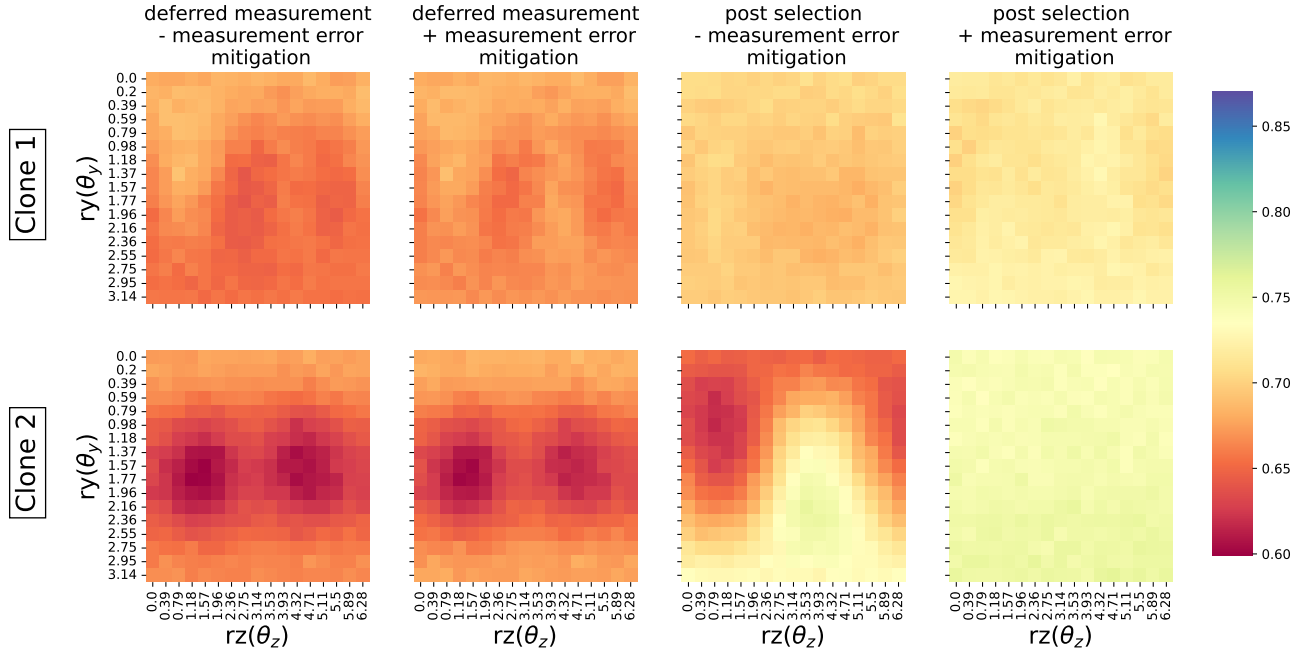


Figure 3: APCC circuit implemented in the form of deferred measurement and post selection of `ibmq_montreal`. The maximum fidelity is 0.833. First and third column show the raw fidelity results without measurement error mitigation, and the second and fourth columns show the same results with measurement error mitigation applied. Run on qubits `0, 2, 1, 4, 7` on `ibmq_montreal`. The qubit clone indices, for the logical circuit, are `0, 3` for APCC deferred measurement and `3, 4` for APCC post selection. The clone numbering on the rows corresponds to this numbering order (in other words the clone number is index based).

can be computed. As an example, the CNOT cost of AAPCCC ($M = 3$) implemented with deferred measurement on the LNN connectivity is: $2M^2 - M + 2(2.5M^2 - 5.5M + 3) + 1 + 4M - 1 = 45$.

Lastly, we give interactive Quirk circuits [21] for our $1 \rightarrow 2$ Telecloning and $1 \rightarrow 3$ Telecloning circuits (with and without ancilla). In these circuits the state of the message qubit is being varied over time. Note that with ancilla, the clones' mixed state & fidelity is independent from the outcome of the Bell measurement of the Message & Port qubits, and without ancilla, the clones mixed state & fidelity is averaged over different mixed states & fidelities depending on the outcome from the Bell measurements. The outcome of the SWAP test relates to the fidelity measure as $(\text{fidelity}) = 1 - 2(\text{ON percentage})$: [1 \$\rightarrow\$ 2 Telecloning Variants](#), [1 \$\rightarrow\$ 3 Telecloning Variants](#).

2.2 Hardware implementation details

In this section the workflow of analyzing and executing the quantum telecloning implementations is described.

Quantum state tomography in general can be computationally intensive, however in this case we are only performing state tomography on single qubits. In order to reduce Quantum Processing Unit (QPU) time usage, we implement single qubit parallel state tomography. This is where the state tomography operations are applied to the clone qubits on the same circuit; therefore the required number of circuits to compute the state tomography of M clone qubits is always 3 (one for each of the three Pauli basis states X/Y/Z). In order to compute the density matrices of the clones, we use the maximum likelihood estimation quantum tomography fitter that is implemented (with slight modifications) in Qiskit Ignis [41, 43]. Once the density matrices of the clones have been constructed, we compute exactly the original density matrix of the message qubit given the known single qubit gates we have applied to initialize the message qubit in the experiments. Then we use Equation 2 in order to compute the *fidelity* [26] of the clone(s) in comparison to the pure quantum state of the message qubit.

$$F(\rho_1, \rho_2) = \text{Tr}[\sqrt{\sqrt{\rho_1}\rho_2\sqrt{\rho_1}}]^2 \quad (2)$$

Note that since the message qubit is a pure state (given the pure state is $\rho_1 = |\psi_1\rangle\langle\psi_1|$), Equation 2 simplifies to Equation 3:

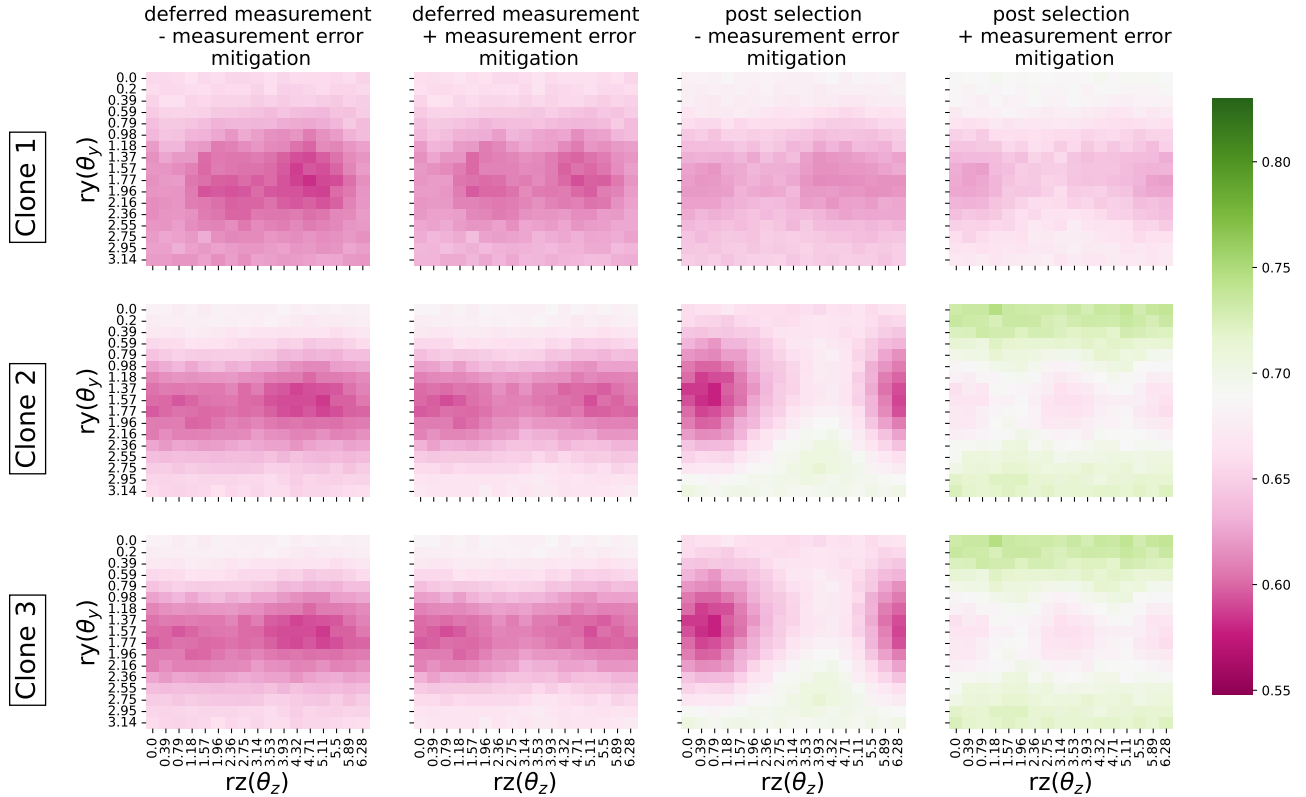


Figure 4: PCCC circuit implemented in the form of deferred measurement and post selection of `ibmq_montreal`. The maximum fidelity is $0.7\bar{7}$. First and third column show the raw fidelity results without measurement error mitigation, and the second and fourth columns show the same results with measurement error mitigation applied. Run on qubits **0, 1, 4, 7, 10** on `ibmq_montreal`. The qubit clone indices, for the logical circuit, are 0, 1, 3 for PCCC deferred measurement and 2, 3, 4 for PCCC post selection. The clone numbering on the rows corresponds to this numbering order (in other words the clone number is index based).

$$F(\rho_1, \rho_2) = \langle \psi_1 | \rho_2 | \psi_1 \rangle \quad (3)$$

In practice we need to estimate the state of the clones using state tomography, and the combination of the least squares estimation process and statistical noise due to a finite number of samples, can result in fidelities which are slightly larger than the theoretical limit given by Equation 1.

Importantly, for all three variants of the quantum telecloning circuits, the delineation between **1**) the telecloning state construction, **2**) the Bell measurement on the message qubit by the telecloning state, and lastly **3**) the parallel state tomography is essential. In order to encode this separation between the components of the telecloning circuits, the **barrier** operation is used. Specifically, two barriers are always present to separate the three telecloning protocol components, although in some cases the measurements are also immediately preceded by a third barrier.

In order to improve the clone fidelity, we implement measurement error mitigation on the IBMQ results using Qiskit Ignis [17, 39]. This technique has been utilized in previous studies in order to obtain higher quality results on NISQ devices [1, 2]. The full measurement error mitigation procedure involves creating and running 2^m circuits which are all possible combinations of X gates or Identity gates (i.e. no gates) on each qubit followed by m measurements on the specific qubit subset being addressed. This then gives a full mapping of the intended prepared states to the measured states on the device. It is then possible to use this mapping to remove some of the measurement error from different executed circuits (in our cases quantum telecloning circuits) that have a similar measurement error profile [39]. Therefore, ideally this measurement error characterization would be run in sequence with the relevant job that we want to reduce the measurement error on. In our case, we run all varying message qubit state circuits and all measurement error mitigation circuits (for that specific qubit subset) in the same job. The disadvantage of the measurement error mitigation procedure is that it is not scalable to a large number of

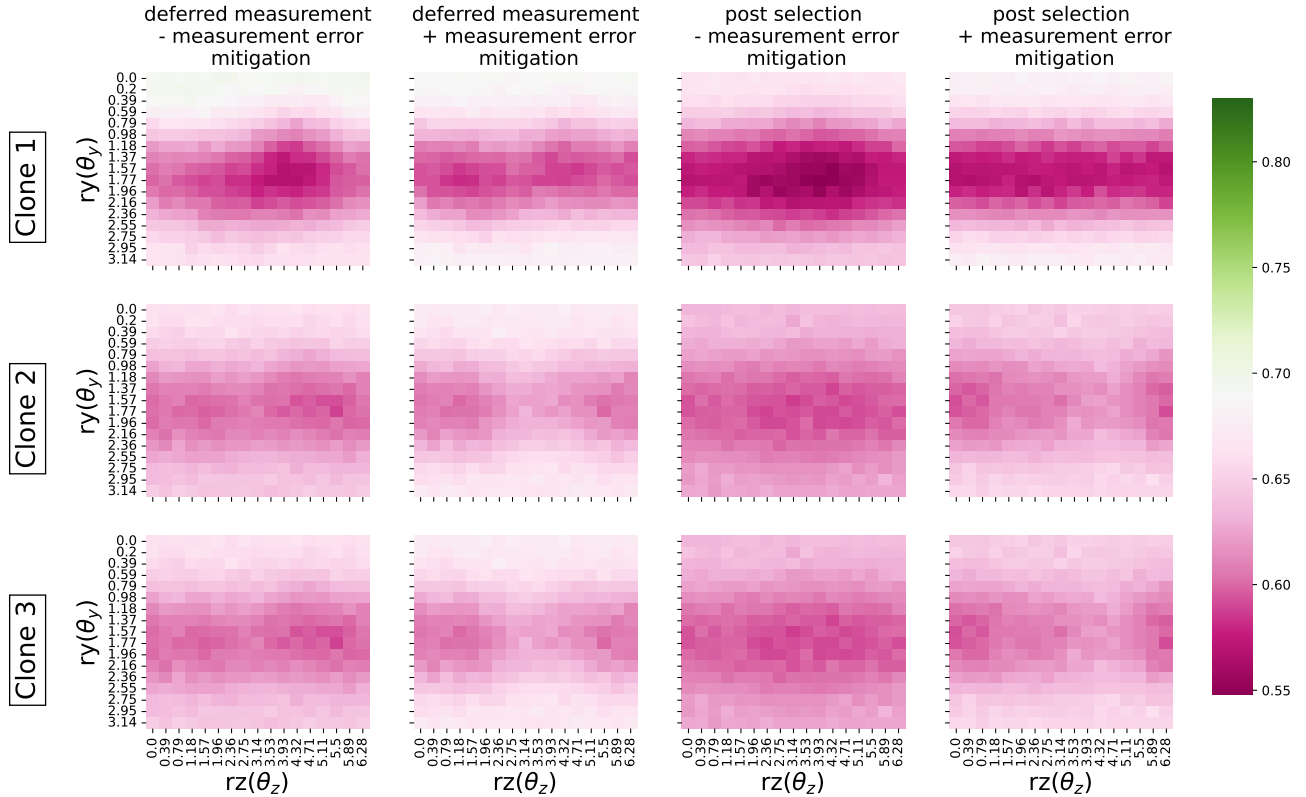


Figure 5: AAPCCC circuit implemented in the form of deferred measurement and post selection of `ibmq_montreal`. The maximum fidelity is $0.7\bar{7}$. First and third column show the raw fidelity results without measurement error mitigation, and the second and fourth columns show the same results with measurement error mitigation applied. Run on qubits **9, 3, 5, 8, 11, 14, 16** on `ibmq_montreal`. The qubit clone indices, for the logical circuit, are 0, 3, 5 for AAPCCC deferred measurement and 4, 5, 6 for AAPCCC post selection. The clone numbering on the rows corresponds to this numbering order (in other words the clone number is index based).

measured qubits, however for our experiments the largest number of circuit measurements is 5 (in the cases of post selection for PCCC and AAPCCC) which requires 32 measurement error mitigation circuits.

We applied the Qiskit transpiler [43] with optimization level set to 3 to all of the circuits submitted to the IBMQ backends. Optimization level 3 is the highest level offered by the transpiler. Besides the circuit optimization in terms of gate depth, the Qiskit transpiler maps the logical circuit qubits onto physical qubits and converts all gates into the IBMQ basis gates **rz**, **sx**, **x**, **cx**; which prepares the circuits for direct submission to the backend. The use of the Qiskit transpiler here did not reduce the CNOT counts in the telecloning circuits (see Section 2.1), although it did reduce the number of single qubit gates after the logical circuits were represented in the IBMQ native gateset.

The primary characterization we measure is how the fidelity between the pure state of the message qubit and M clones changes as a function of the message qubit state that is being cloned. To this end, the message qubit state is parameterized by two angles; θ_y and θ_z , which correspond to the single qubit gates **ry** and **rz** applied in sequence (as in Figure 1): $ry(\theta_y)$, $rz(\theta_z)$. On the IBMQ experiments the angles were varied from $\theta_y \in [0, \pi]$ and $\theta_z \in [0, 2\pi]$. For both θ_y and θ_z we create 17 linearly spaced (inclusive) angles to vary the message qubit state over, resulting in 289 message qubit states.¹ Then each of these circuits are run 3 times for each of the three Pauli basis states for the state tomography estimation [41, 43]; therefore the total number of telecloning circuits is 867. Additionally, we run measurement error mitigation circuits in the same job as the quantum telecloning circuits. As an example, for a deferred measurement PCC job submission the final number of circuits combined into a single job is $867 + 2^2 = 871$. However, for a post selection PCCC job submission, the total number of circuits combined

¹Note that the linearly spaced angles are strictly not a geometrically accurate representation of the Bloch sphere, but it suffices for the purpose of characterizing the algorithm and hardware performance on the quantum telecloning circuits.

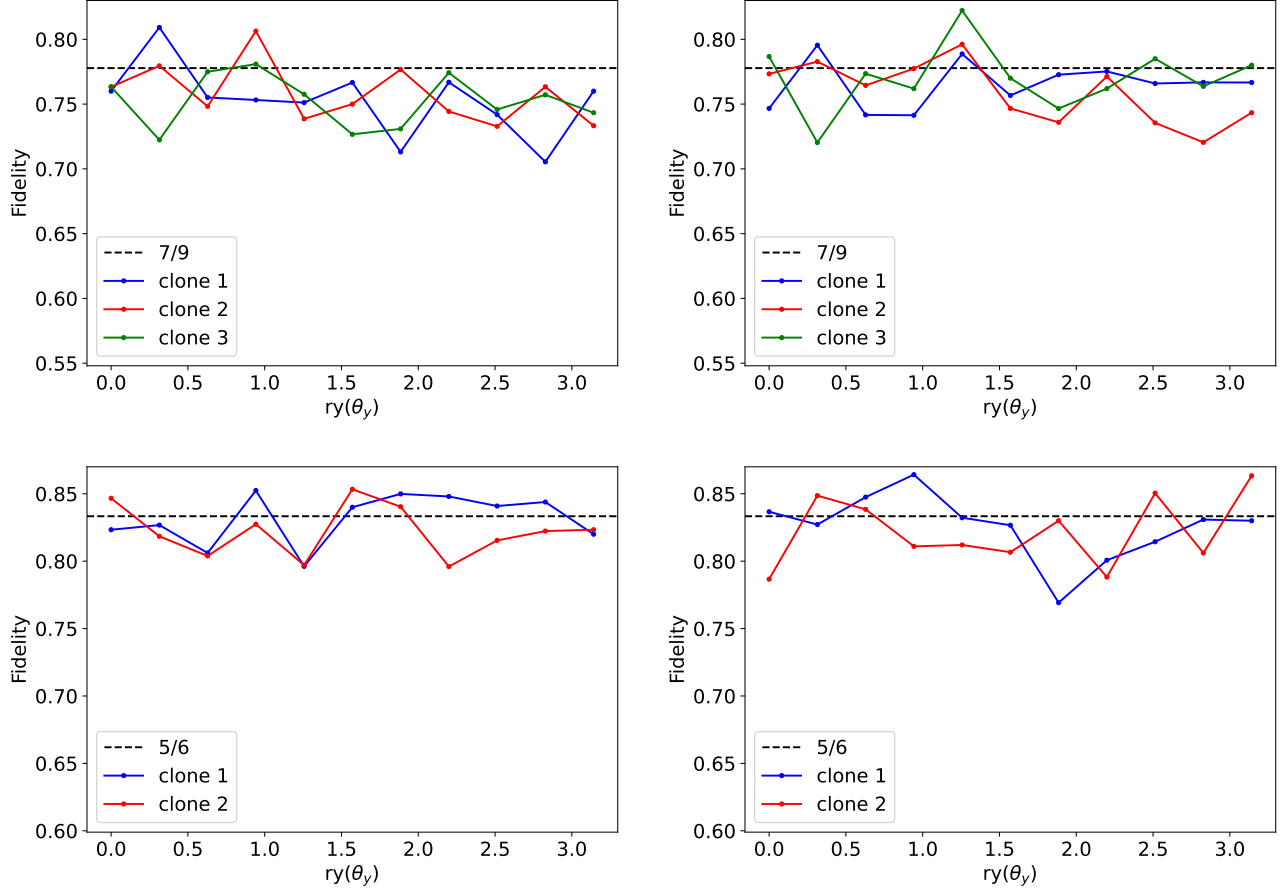


Figure 6: Measured fidelity values as a function of θ_y ($\theta_z = \frac{\pi}{2}$) for the AAPCC (upper left), PCCC (upper right), APCC (lower left), and PCC (lower right) circuits with mid-circuit measurement and real time classical if statements implemented on Quantinuum H1-2. The maximum fidelity for 2 and 3 clones is $0.8\overline{33}$ and $0.7\overline{7}$ respectively.

into a single job is $867 + 2^5 = 899$. The `ibmq_montreal` and `ibmq_toronto` backends are currently the two IBMQ devices which allow the largest number of circuits to be submitted in a single job across all IBMQ devices; that limit is 900 circuits per job. Each post selection state (which constitutes a different circuit for each state) is run separately, but with its own measurement error mitigation circuits. Therefore, this methodology fits within the provided system constraints. It is important to run all circuits within the same time span in order to attempt to mitigate the effects of noise drift and to get consistent results. All IBMQ circuits used 30,000 shots per circuit in order to get statistically robust sample sizes.

For the post selection implementation, in order to compute the fidelity of each clone qubit, the results are first filtered for the post-selected states, and then the counts of 0 and 1 measurements for each clone qubit (measured using parallel state tomography) are summed across the 4 post-selection states. Then a single fidelity value is computed using the sum of the post selected states. Interestingly, the proportion of post-selection results which are kept for each bitstring varies between the PCC and APCC circuit implementations; the APCC circuit implementation have an ideal proportion that is kept of 0.25 for each of the 4 classical results. Whereas the PCC circuit implementation has post selected samples proportion that varies between $\frac{1}{3}$ and $\frac{1}{6}$. This is further examined in the experimental results in Section 3.1.

For running on the Quantinuum H1-2 backend 11 linearly spaced θ_y angles over $[0, \pi]$ were used, along with a fixed $rz(\frac{\pi}{2})$ gate. Each circuit (still using parallel state tomography) was run using 300 shots. The small number of shots is due to usage limitations in place on the Quantinuum system. Measurement error mitigation was not used on the H1-2 jobs. By default, the Quantinuum backend applies some circuit optimizations in the process of compiling the user-submitted circuit to the device hardware; this flag is left on when executing circuits.

3 Results

In this section we describe the measured fidelities of the different quantum telecloning implementation variants run on both IBMQ and Quantinuum NISQ computers.

The fidelity results can vary significantly, and in order to appropriately show the relative fidelity values achieved, we have scaled the figures into the same fidelity ranges (in terms of either fidelity axis or heatmap values) for two clone figures and three clone figures. The reason for this differentiation between the different clone numbers is that the theoretical clone fidelity decreases for larger values of M (see Equation 1).

Figure 2 shows the measured fidelity values in the form of a heatmap for the deferred measurement and post selection variants of the PCC circuit, run on `ibmq_montreal`. The column headers show that with measurement error mitigation the clone fidelities improve on average, although in some cases (for example the deferred measurement) the differences seem quite small. The row headers label the index of the clone qubit in the circuit. We expect post selection to perform better on average than deferred measurement, which we observe to be the case. We also expect that post selection in conjunction with measurement error mitigation would perform the best overall, which is the case in Figure 2. Post selection with measurement error mitigation consistently approaches and even reaches the theoretical limit of $\frac{5}{6}$.

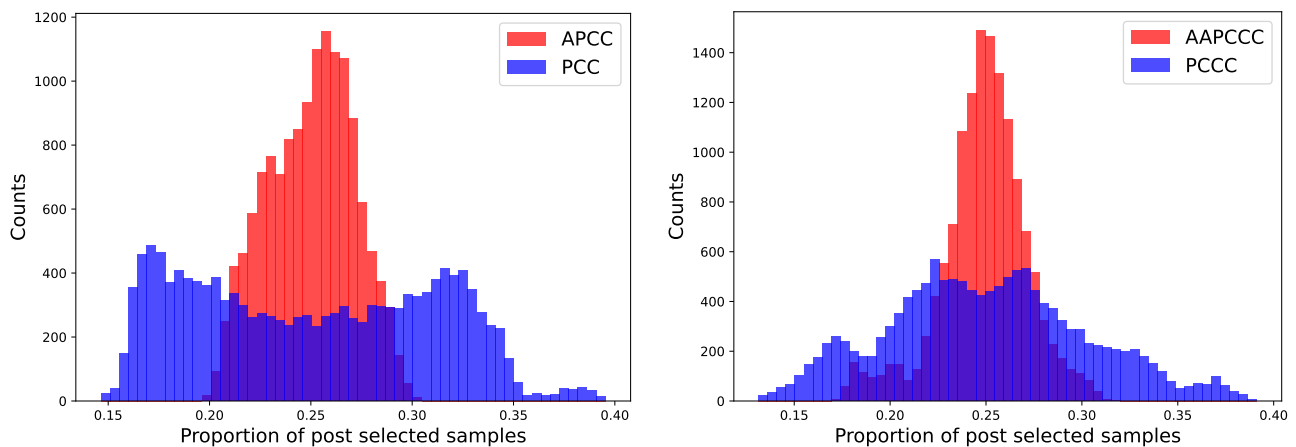


Figure 7: Post selection count histograms for two clone circuits (left hand) and three clone circuits (right hand) across 4 separate runs of each circuit on different qubit layouts of `ibmq_montreal`. These are the raw circuit measurement counts, not corrected by the measurement error mitigation procedure.

Figure 3 shows the measured fidelity values for the APCC circuit and is structured in an identical manner to Figure 2, where columns are the deferred measurement and post selection implementations with and without measurement error mitigation, and the rows are the two clone indices. These circuits were also run on `ibmq_montreal`. The APCC circuit uses more gates and more qubits than the PCC circuit, therefore we expect the PCC circuit to have higher fidelity on average than the APCC circuit. Comparing Figure 2 and 3, this appears to be the case. As with the PCC circuit, the measurement error mitigation improves fidelity on average and the post selection circuits have higher fidelity than the deferred measurement circuits.

In order to visually differentiate the two clone heatmaps (Figures 3 and 2) from the three clone heatmaps (Figures 5 and 4), two different color gradients are used. Figure 4 shows the fidelity values for the PCCC circuit. The figure is structured in the same way to the previous two fidelity heatmap figures, but it now also includes the third clone fidelities. Notice that the heatmap scales are consistent with the other three clone results in Figure 5 and Figure 6. As with the two clone circuits, we observe that post selection with measurement error mitigation achieves better fidelity results on average. In particular, these fidelity values are approaching, although not quite reaching, the theoretical limit of $0.7\bar{7}$. As expected, deferred measurement has poorer fidelity than post selection. Measurement error mitigation consistently improves the measured fidelities as well.

Figure 5 shows the fidelity values for the AAPCCC telecloning circuit. This circuit is the largest of the telecloning circuits we have run, both in terms of number of qubits, number of measurements, and number of gates. Therefore, the relatively low fidelity values across most of the implementations is not unexpected. Although it is encouraging that the fidelity values are approaching 0.70 in some cases.

Interestingly, Figures 2, 3, 4 and 5 all show clear clusters and patterns of fidelity (or infidelity). In particular,

this seems to show that the clone fidelity of the universal quantum telecloning circuits are state *dependent* when implemented on the IBMQ hardware (however, the logical circuits themselves are universal, meaning state *independent*). The exact cause of this mechanism is not known, but it could be because of asymmetry in the quantum control mechanisms or persistent environmental noise. Similar trends in single qubit fidelity have been investigated before on IBMQ hardware [42] and the telecloning process could be cloning the already slightly decoherent message qubit (which may decohere or be prepared in an unintentionally state dependent manner).

Figure 6 shows the fidelity (y-axis) results for varying ry angles (x-axis) in the range $[0, \pi]$ for the PCC, APCC, PCCC, and AAPCCC circuits implemented on the Quantinuum H1-2 device. The fidelity results are consistently approaching the theoretical clone fidelity values. These high fidelity results with no error mitigation can be attributed to the low error rates and all-to-all connectivity of the H1-2 device.

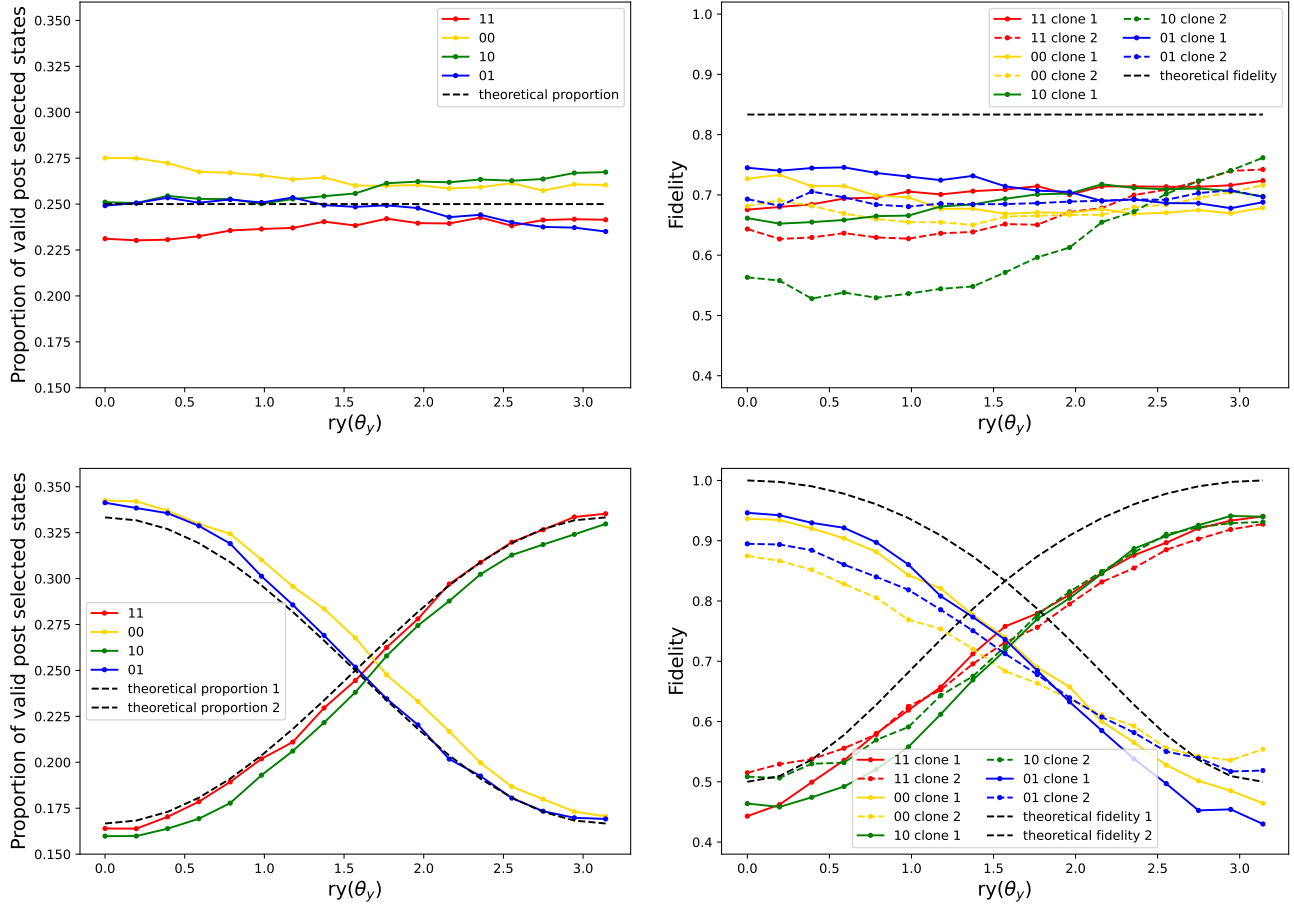


Figure 8: A more detailed analysis of post selection results in terms of samples kept after post selection and fidelity for each of those post selected state samples (no measurement error mitigation). The x-axis is varying $\theta_y \in [0, \pi]$, and $\theta_z = \frac{\pi}{2}$. Top row shows results from the APCC circuit, and the bottom row shows results from the PCC circuit. Left hand column shows the proportion of samples which were kept after post selection. Right hand column shows the fidelity results for the post selection experiments split by the 4 post selection states (as well as by clone number). These results come from a subset of the post selection experiments shown in Figures 2 and 3.

3.1 Post selection characteristics

Figure 7 shows the distribution of post selection states for PCC, APCC, PCCC, and AAPCCC circuits. The total number of datapoints being plotted in each distribution is 13872². The APCC distribution is expected to

²13872 comes from 3 parallel state tomography circuits, 17 θ_y and θ_z angles, 4 post selection states, and 4 different hardware implementations: $3 \cdot 17 \cdot 17 \cdot 4 \cdot 4 = 13872$

be approximately binomial with a mean at 0.25. The wide variance observed is due to the overall noise from implementation on the NISQ hardware.

Figure 8 shows the post selection state proportion and fidelity for each post selection state as a function of ry of the message qubit. Notably the proportion of samples which are kept after post selection are relatively consistent with the (expected) theoretical values. The two possible ideal post selection proportions for the PCC circuit are given in Equation 4 and the two possible ideal post selected fidelities for the PCC circuit are given by Equation 5. Notably, the theoretical curves and the experimental curves for PCC intersect at the same post selection proportion, and the fidelity results also intersect at the expected angle of $\frac{\pi}{2}$ although at a lower fidelity value than the theoretical curves (which is consistent with the fidelity results in Figures 3 and 2).

$$\frac{1}{6}[2\cos(\frac{\theta}{2})^2 + \sin(\frac{\theta}{2})^2]$$

$$\frac{1}{6}[\cos(\frac{\theta}{2})^2 + 2\sin(\frac{\theta}{2})^2]$$
(4)

$$\frac{(4\cos(\frac{\theta}{2})^2 + \sin(\frac{\theta}{2})^2)}{2(2\cos(\frac{\theta}{2})^2 + \sin(\frac{\theta}{2})^2)}$$

$$\frac{(\cos(\frac{\theta}{2})^2 + 4\sin(\frac{\theta}{2})^2)}{2(\cos(\frac{\theta}{2})^2 + 2\sin(\frac{\theta}{2})^2)}$$
(5)

Figures 7 and 8 show that the proportion of post selected states for PCC varies between $\frac{1}{6}$ and $\frac{1}{3}$, while for APCC it is $\frac{1}{4}$. The measured fidelity for each post selection experiment is effectively a weighted sum (weighted by the proportion of post selected states) of the fidelities for each post selection state.

4 Conclusion

In this work we demonstrated the viability of performing an emulation of quantum telecloning on NISQ computers. The most direct method of performing quantum telecloning on a gate model quantum computer is to perform the necessary bell measurement during circuit execution, and then use real time classical conditional control in order to generate the clones in real time. We demonstrate that this is possible on the Quantinuum H1-2 device. In cases where this feature is not present, we show that alternative methods such as deferred measurement and post selection allow for analysis of the telecloning protocol. We also present a novel $1 \rightarrow 3$ telecloning quantum circuit with no ancilla. Importantly, with the use of measurement error mitigation in the case of deferred measurement and post selection on the IBMQ devices, the clone fidelities can approach the theoretical fidelity limit. The low error rate and all-to-all connectivity of the Quantinuum H1-2 device cause correspondingly high fidelity values which are consistently close to the theoretical fidelity limit.

There are numerous research avenues that are left for future research:

- Given the availability of cloud based NISQ platforms, is there meaningful quantum cryptographic analysis or experimental quantum network protocol implementations that can be done on these devices?
- Is there a scalable quantum telecloning algorithm that can be developed to move from 2 and 3 clone circuits to $M \geq 4$ clones with no ancilla?
- How do telecloning circuits (with ancilla) with clones ≥ 3 perform on current NISQ devices?
- The related idea of remote information concentration protocols could also be implemented on gate model NISQ computers [32, 46].

5 Acknowledgments

We acknowledge the use of IBM Quantum services for this work. The views expressed are those of the authors, and do not reflect the official policy or position of IBM or the IBM Quantum team.

This research used resources of the Oak Ridge Leadership Computing Facility, which is a DOE Office of Science User Facility supported under Contract DE-AC05-00OR22725.

Research presented in this article was supported by the Laboratory Directed Research and Development program of Los Alamos National Laboratory under project number 20220656ER. LA-UR-22-23967

The authors thank Adrien Suau for helpful discussions on single qubit tomography.

References

- [1] Shamminuj Aktar, Andreas Bäertschi, Abdel-Hameed A. Badawy, and Stephan Eidenbenz. A divide-and-conquer approach to dicke state preparation, 2021. URL: <https://arxiv.org/abs/2112.12435>, doi:10.48550/ARXIV.2112.12435.
- [2] Thomas Alexander, Naoki Kanazawa, Daniel J Egger, Lauren Capelluto, Christopher J Wood, Ali Javadi-Abhari, and David C McKay. Qiskit pulse: programming quantum computers through the cloud with pulses. *Quantum Science and Technology*, 5(4):044006, 2020.
- [3] Martin Aulbach, Damian Markham, and Mio Muraō. The maximally entangled symmetric state in terms of the geometric measure. *New Journal of Physics*, 12(7):073025, 2010.
- [4] Charles H Bennett and Gilles Brassard. Proceedings of the iee international conference on computers, systems and signal processing, 1984.
- [5] Charles H Bennett, Gilles Brassard, Claude Crépeau, Richard Jozsa, Asher Peres, and William K Wootters. Teleporting an unknown quantum state via dual classical and einstein-podolsky-rosen channels. *Physical review letters*, 70(13):1895, 1993.
- [6] Samuel L. Braunstein, Vladimír Bužek, and Mark Hillery. Quantum-information distributors: Quantum network for symmetric and asymmetric cloning in arbitrary dimension and continuous limit. *Physical Review A*, 63(5), apr 2001. URL: <https://doi.org/10.1103/PhysRevA.63.052313>, doi:10.1103/physreva.63.052313.
- [7] Dagmar Bruß, David P DiVincenzo, Artur Ekert, Christopher A Fuchs, Chiara Macchiavello, and John A Smolin. Optimal universal and state-dependent quantum cloning. *Physical Review A*, 57(4):2368, 1998.
- [8] V. Bužek, S. L. Braunstein, M. Hillery, and D. Bruß. Quantum copying: A network. *Phys. Rev. A*, 56:3446–3452, Nov 1997. URL: <https://link.aps.org/doi/10.1103/PhysRevA.56.3446>, doi:10.1103/PhysRevA.56.3446.
- [9] Adam Burchardt, Jakub Czartowski, and Karol Życzkowski. Entanglement in highly symmetric multipartite quantum states. *Physical Review A*, 104(2), aug 2021. URL: <https://doi.org/10.1103/PhysRevA.104.022426>, doi:10.1103/physreva.104.022426.
- [10] Vladimir Bužek and Mark Hillery. Quantum copying: Beyond the no-cloning theorem. *Physical Review A*, 54(3):1844, 1996.
- [11] Vladimir Buzek and Mark Hillery. Universal optimal cloning of qubits and quantum registers, 1998. URL: <https://arxiv.org/abs/quant-ph/9801009>, doi:10.48550/ARXIV.QUANT-PH/9801009.
- [12] Andreas Bäertschi and Stephan Eidenbenz. Deterministic preparation of dicke states. In *Fundamentals of Computation Theory*, pages 126–139. Springer International Publishing, 2019. URL: https://doi.org/10.1007/978-3-030-25027-0_9, doi:10.1007/978-3-030-25027-0_9.
- [13] N. J. Cerf, A. Ipe, and X. Rottenberg. Cloning of continuous quantum variables. *Phys. Rev. Lett.*, 85:1754–1757, Aug 2000. URL: <https://link.aps.org/doi/10.1103/PhysRevLett.85.1754>, doi:10.1103/PhysRevLett.85.1754.
- [14] Nicolas J. Cerf. Pauli cloning of a quantum bit. *Phys. Rev. Lett.*, 84:4497–4500, May 2000. URL: <https://link.aps.org/doi/10.1103/PhysRevLett.84.4497>, doi:10.1103/PhysRevLett.84.4497.
- [15] Lin Chen and Yi-Xin Chen. Asymmetric quantum telecloning of multiqubit states. *Quantum Info. Comput.*, 7(8):716–729, nov 2007.

- [16] A. Chiuri, C. Greganti, M. Paternostro, G. Vallone, and P. Mataloni. Experimental quantum networking protocols via four-qubit hyperentangled dicke states. *Phys. Rev. Lett.*, 109:173604, Oct 2012. URL: <https://link.aps.org/doi/10.1103/PhysRevLett.109.173604>, doi:10.1103/PhysRevLett.109.173604.
- [17] Andreas Dewes, Florian R Ong, Vivien Schmitt, R Lauro, N Boulant, P Bertet, D Vion, and D Esteve. Characterization of a two-transmon processor with individual single-shot qubit readout. *Physical review letters*, 108(5):057002, 2012.
- [18] R. H. Dicke. Coherence in spontaneous radiation processes. *Phys. Rev.*, 93:99–110, Jan 1954. URL: <https://link.aps.org/doi/10.1103/PhysRev.93.99>, doi:10.1103/PhysRev.93.99.
- [19] Lu-Ming Duan and Guang-Can Guo. Probabilistic cloning and identification of linearly independent quantum states. *Physical review letters*, 80(22):4999, 1998.
- [20] Tim M Forcer, Anthony JG Hey, DA Ross, and PGR Smith. Superposition, entanglement and quantum computation. *Quantum Inf. Comput.*, 2(2):97–116, 2002.
- [21] Craig Gidney. Quirk: Quantum Circuit Simulator. A drag-and-drop quantum circuit simulator. URL: <https://algassert.com/quirk>.
- [22] N Gisin and H Bechmann-Pasquinucci. Bell inequality, bell states and maximally entangled states for n qubits. *Physics Letters A*, 246(1-2):1–6, sep 1998. URL: <https://doi.org/10.1016%2Fs0375-9601%2898%2900516-7>, doi:10.1016/s0375-9601(98)00516-7.
- [23] Nicolas Gisin and Serge Massar. Optimal quantum cloning machines. *Physical review letters*, 79(11):2153, 1997.
- [24] O. Gühne, F. Bodoky, and M. Blaauuboer. Multiparticle entanglement under the influence of decoherence. *Physical Review A*, 78(6), dec 2008. URL: <https://doi.org/10.1103%2Fphysreva.78.060301>, doi:10.1103/physreva.78.060301.
- [25] S. Iblisdir, A. Acín, N. J. Cerf, R. Filip, J. Fiurášek, and N. Gisin. Multipartite asymmetric quantum cloning. *Physical Review A*, 72(4), oct 2005. URL: <https://doi.org/10.1103%2Fphysreva.72.042328>, doi:10.1103/physreva.72.042328.
- [26] Richard Jozsa. Fidelity for Mixed Quantum States. *Journal of Modern Optics*, 41(12):2315–2323, 1994. doi:10.1080/09500349414552171.
- [27] Richard Jozsa. Entanglement and quantum computation, 1997. URL: <https://arxiv.org/abs/quant-ph/9707034>, doi:10.48550/ARXIV.QUANT-PH/9707034.
- [28] Alastair Kay. Quantikz: A tikz library to typeset quantum circuit diagrams. Tutorial on the Quantikz Package. [arXiv:1809.03842](https://arxiv.org/abs/1809.03842), doi:10.17637/rh.7000520.
- [29] Seth Lloyd and Samuel L. Braunstein. Quantum computation over continuous variables. *Physical Review Letters*, 82(8):1784–1787, feb 1999. URL: <https://doi.org/10.1103%2Fphysrevlett.82.1784>, doi:10.1103/physrevlett.82.1784.
- [30] M. Murao, D. Jonathan, M. B. Plenio, and V. Vedral. Quantum telecloning and multiparticle entanglement. *Phys. Rev. A*, 59:156–161, Jan 1999. URL: <https://link.aps.org/doi/10.1103/PhysRevA.59.156>, doi:10.1103/PhysRevA.59.156.
- [31] Mio Murao, Martin B. Plenio, and Vlatko Vedral. Quantum-information distribution via entanglement. *Phys. Rev. A*, 61:032311, Feb 2000. URL: <https://link.aps.org/doi/10.1103/PhysRevA.61.032311>, doi:10.1103/PhysRevA.61.032311.
- [32] Mio Murao and Vlatko Vedral. Remote information concentration using a bound entangled state. *Phys. Rev. Lett.*, 86:352–355, Jan 2001. URL: <https://link.aps.org/doi/10.1103/PhysRevLett.86.352>, doi:10.1103/PhysRevLett.86.352.
- [33] Michael A Nielsen and Isaac L Chuang. Quantum computation and quantum information, 2000.

- [34] Chi-Sheng Niu and Robert B. Griffiths. Optimal copying of one quantum bit. *Physical Review A*, 58(6):4377–4393, dec 1998. URL: <https://doi.org/10.1103/PhysRevA.58.4377>, doi:10.1103/physreva.58.4377.
- [35] Arun Kumar Pati. Quantum superposition of multiple clones and the novel cloning machine. *Physical review letters*, 83(14):2849, 1999.
- [36] Juan M Pino, Jennifer M Dreiling, Caroline Figgatt, John P Gaebler, Steven A Moses, MS Allman, CH Baldwin, M Foss-Feig, D Hayes, K Mayer, et al. Demonstration of the trapped-ion quantum ccd computer architecture. *Nature*, 592(7853):209–213, 2021.
- [37] John Preskill. Quantum Computing in the NISQ era and beyond. *Quantum*, 2:79, August 2018. doi:10.22331/q-2018-08-06-79.
- [38] Wang Qiong, Li Ji-Xin, and Zang Hao-Sheng. Symmetric telecloning and entanglement distribution of spin quantum states. *Chinese Physics Letters*, 25(8):2770–2773, jul 2008. doi:10.1088/0256-307x/25/8/010.
- [39] Qiskit. Measurement error mitigation. <https://qiskit.org/textbook/ch-quantum-hardware/measurement-error-mitigation.html>, April 2022.
- [40] Valerio Scarani, Sofyan Iblisdir, Nicolas Gisin, and Antonio Acin. Quantum cloning. *Reviews of Modern Physics*, 77(4):1225, 2005.
- [41] John A. Smolin, Jay M. Gambetta, and Graeme Smith. Efficient method for computing the maximum-likelihood quantum state from measurements with additive gaussian noise. *Phys. Rev. Lett.*, 108:070502, Feb 2012. URL: <https://link.aps.org/doi/10.1103/PhysRevLett.108.070502>, doi:10.1103/PhysRevLett.108.070502.
- [42] Adrien Suau, Marc Vuffray, Andrey Y. Lokhov, Lukasz Cincio, and Carleton Coffrin. Vector field visualization of single-qubit state tomography. 2022.
- [43] Matthew Treinish, Jay Gambetta, Paul Nation, Paul Kassebaum, qiskit bot, Diego M. Rodríguez, Salvador de la Puente González, Shaohan Hu, Kevin Krsulich, Laura Zdanski, Jessie Yu, Jim Garrison, Julien Gacon, David McKay, Juan Gomez, Lauren Capelluto, Travis-S-IBM, Manoel Marques, Ashish Panigrahi, lerongil, Rafey Iqbal Rahman, Steve Wood, Luciano Bello, Divyanshu Singh, Drew, Eli Arbel, Joachim Schwarm, Jonathan Daniel, MELVIN GEORGE, and Omar Costa Hamido. Qiskit/qiskit: Qiskit 0.34.1, January 2022. doi:10.5281/zenodo.5823346.
- [44] P. van Loock and Samuel L. Braunstein. Telecloning of continuous quantum variables. *Phys. Rev. Lett.*, 87:247901, Nov 2001. URL: <https://link.aps.org/doi/10.1103/PhysRevLett.87.247901>, doi:10.1103/PhysRevLett.87.247901.
- [45] Qingwei Wang, Wei Li, Yimiao Wu, Wenxiu Yao, Fan Li, Long Tian, Yajun Wang, and Yaohui Zheng. Demonstration of $1 \rightarrow 3$ continuous-variable quantum telecloning. *Phys. Rev. A*, 104:032419, Sep 2021. URL: <https://link.aps.org/doi/10.1103/PhysRevA.104.032419>, doi:10.1103/PhysRevA.104.032419.
- [46] Xin-Wen Wang, Shi-Qing Tang, Li-Jun Xie, Deng-Yu Zhang, and Le-Man Kuang. Many-to-one remote information concentration for qudits and multipartite entanglement, 2013. arXiv:1302.0626.
- [47] William K Wootters and Wojciech H Zurek. A single quantum cannot be cloned. *Nature*, 299(5886):802–803, 1982.
- [48] Zhi Zhao, An-Ning Zhang, Xiao-Qi Zhou, Yu-Ao Chen, Chao-Yang Lu, Anders Karlsson, and Jian-Wei Pan. Experimental realization of optimal asymmetric cloning and telecloning via partial teleportation. *Physical Review Letters*, 95(3), jul 2005. URL: <https://doi.org/10.1103/PhysRevLett.95.030502>, doi:10.1103/physrevlett.95.030502.
- [49] Yang Zhen, Zhang Wen-Hai, He Juan, and Ye Liu. Scheme to implement optimal symmetric $1 \rightarrow 2$ universal quantum telecloning through cavity-assisted interaction. *Communications in Theoretical Physics*, 50(5):1096–1100, nov 2008. doi:10.1088/0253-6102/50/5/17.